JOURNAL OF MATERIALS SCIENCE 28 (1993) 5852–5862

Effect of hydrolysis time and type of catalyst on the stability of tetragonal zirconia–silica composites synthesized from alkoxides

G. MONRÓS, M.C. MARTÍ, J. CARDA, M.A. TENA, P. ESCRIBANO
Dpt. Ciències Experimentals, Àrea Química Inorgànica, Universitat Jaume I, Castelló, Spain
M. ANGLADA
Dpt. de Ciència dels Materials i Enginyeria Metallúrgica, Universitat Politècnica de Catalunya, Barcelona, Spain

ZrO_2-transformation-toughened glass-ceramics have been prepared by the sol–gel process from either colloidal gels (CG) or polymeric gels from alkoxides (PG), using, in the latest method, a different catalyst (acid, basic and without catalyst), and different compositions in the $ZrO_2 \cdot SiO_2$ system (free ZrO_2 included). The different methods of synthesis of tetragonal zirconia in SiO_2 matrix were compared in order to obtain thermal stability, and a high amount of stabilized tetragonal zirconia. The effect of catalyst, hydrolysis time, chemical composition, critical particle size in $ZrO_2(t) \rightarrow ZrO_2(m)$ transformation, the doping with vanadium on the $ZrO_2(t)$ stability in SiO_2 matrix and Vickers microhardness of samples have also been studied.

1. Introduction

Ceramic composites have recently attracted high interest and study, particularly composites for improved mechanical behaviour. They have resulted in mechanical properties that were felt improbable or not thought of 5–15 years ago. Ceramic composites are an outstanding example of both the need for, and the results achievable from, applying more sophisticated chemistry to their processing [1].

Zirconia has classically received attention because of its superior properties of mechanical strength. The polymorphic nature of pure zirconia is well known: the cubic phase (fluorite structure, space group $Fm3m$) is stable from the melting point, 2680 °C, to 2370 °C. Between 2370 and 1170 °C, a tetragonally distorted fluorite structure (space group, $P42/nmc$) is stable; below 1170 °C, a further distortion towards monoclinic symmetry (space group $P21/c$) occurs. More recently, an orthorhombic polymorph has been reported; this polymorph appears at low temperature or by the action of stress [2].

The tetragonal–monoclinic ($ZrO_2(t) \rightarrow ZrO_2(m)$) phase transformation has received much attention, because the anisotropic and large (by 3%) volume increase in transformation often causes severe cracking if zirconia-containing ceramics are cycled through the temperature transformation. This fact precludes the use of zirconia as a refractory. However, it is decisive in order of the phenomena of transformation toughening in zirconia [3]. Thus, when the preparation of metastable tetragonal zirconia at room temperature has been successful, the martensitic $ZrO_2(t) \rightarrow ZrO_2(m)$ phase transformation may occur in front of a crack, enhancing toughness just prior to or during its handling. In these cases of stress-induced martensitic transformation, it has been suggested that the phase transformation in front of a crack is equivalent to a non-elastic transformation, and as such it is capable of absorbing the energy that would have otherwise been available for crack extension [4].

Classically, it is possible to stabilize metastable zirconia at room temperature (tetragonal or cubic) by doping with MgO, Y_2O_3 or other alcalinoterrous oxides. When $MgO–ZrO_2$ or $Y_2O_3–ZrO_2$ are fired at adequate temperature, depending on composition, the metastable phase of solid solution precipitates, such as in fully stabilized ZrO_2 (FSZ) with only cubic phase present, partially stabilized ZrO_2 (PSZ) with tetragonal zirconia precipitated into a cubic matrix, or tetragonal zirconia polycrystals (TZP) integrated by small (grain size around 1 μm) monophasic crystals of tetragonal zirconia. Likewise, a two-phase transformation-toughened ceramic is achieved by a mechanism of dispersing zirconia as in a ceramic matrix [5, 6] such as Al_2O_3 or mullite (particulate composites) by the hot-pressing process. More recently, a new method was proposed to prepare ZrO_2-transformation-toughened glass-ceramics by the sol–gel process from metal alkoxides [7].

The following facts concerning two-phase transformation-toughened ceramics based on the $ZrO_2(t) \rightarrow ZrO_2(m)$ transformation, have been reported in the literature.

(a) Martensitic transformation $ZrO_2(t) \rightarrow ZrO_2(m)$ is an adiffusional phase transition. The temperature, M_s, of the martensitic transformation is related to the size of the particles of $ZrO_2(t)$. Namely, as the size of $ZrO_2(t)$ increases, the M_s temperature increases,

0022–2461

becoming higher than room temperature, and the transformation to ZrO_2(m) occurs during cooling. The relationship between M_s and particle size seems to be due to nucleation factors in terms of the different tendency to nucleate the transformation in large and small particles [5].

(b) $ZrO_2(t) \rightarrow ZrO_2(m)$ are thermally activated. The heat-treatment time-required for the transformation was shorter at higher temperature. At high temperature ($> 1200\,^{\circ}C$) the precipitated crystals are predominantly ZrO_2(t) with a small amount of cristobalite in samples from alkoxides [7].

(c) The critical particle size of the ZrO_2(t) free particle is around 30 nm, while the critical particle size of the constrained particle, such as a ZrO_2 particle in Al_2O_3 matrix, is larger, typically ≈ 600 nm. In gels from alkoxides after the $ZrO_2 \cdot SiO_2$ system, even though ZrO_2(t) particles were precipitated in an SiO_2 matrix, the critical particle size was closer to that of the free particle [7].

(d) Elastic deformation strength could be measured by Young's modulus or by Vickers microhardness (HV), and fracture strength by fracture toughness, K_{IC}. The literature on zirconia–silica composites from alkoxides shows [7, 8] an: HV increase with ZrO_2 content and it is maximum for $ZrO_2 \cdot SiO_2$ composition (7.26 GPa in a sample fired at 900 °C with ZrO_2(t) stabilized in a silica matrix [8]); likewise, it increases, when the porosity of the material decreases. A value of $K_{IC} = 4.76\ MPa\,m^{-1/2}$ in $3ZrO_2 \cdot 2SiO_2$ composition fired at 1.100 °C/1 h (HV = 7.57 GPa) is reached, on the other hand, before ZrO_2(t) crystallizes in this sample (800 °C), $K_{IC} = 1.26\ MPa\,m^{-1/2}$ and HV = 6.37 GPa. K_{IC} increases notably with crystallite size of precipitated ZrO_2(t) phase (around 2.5 and $4.5\ MPa\,m^{-1/2}$ from 10 and 20 nm crystallite size, respectively, in $3ZrO_2 \cdot 2SiO_2$ composition).

In the research described here the following aims were proposed in order to attempt a deeper knowledge about the two-phase transformation-toughened ceramics based on the $ZrO_2(t) \rightarrow ZrO_2(m)$ transformation:

(a) to prepare ZrO_2-transformation-toughened glass-ceramics by sol–gel process from either the colloidal gels (CG) or the polymeric gels from alkoxides (PG), using, in the latest method, a different catalyst (acid, basic and without catalyst), and different compositions in the $ZrO_2 \cdot xSiO_2$ system (free ZrO_2 included, $x = 0$);

TABLE I Composition, methods and catalyst employed

	Sample			
	1	2	3	4
ZrO_2 (mol)	100	100	100	96
SiO_2 (mol)	0	50	100	100
V_2O_5 (mol)	0	0	0	2
Method	PG	PG	PG, CG	PG, CG
Catalyst	1–3	1–3	1–3	1–3

Catalyst: (1) HNO_3, (2) NH_3 and (3) without catalyst.

(b) to compare the different methods of synthesis of tetragonal zirconia in the SiO_2 matrix in order to obtain thermal stability, and a high amount of stabilized tetragonal zirconia.

(c) to study the effect of catalyst, hydrolysis time, chemical composition and critical particle size in $ZrO_2(t) \rightarrow ZrO_2(m)$ transformation on the ZrO_2(t) stability in the SiO_2 matrix, and the Vickers microhardness of the samples;

(d) to study the effect of doping with vanadium as the system evolves.

2. Experimental procedure

2.1. Composition of samples and heat treatment

The different compositions and methods used in the preparation of xerogels are shown in Table I. They were fired at temperatures of 300, 600, 700, 750, 800, 900, 1000, 1100, 1200 and 1400 °C successively with 12 h soaking for each firing temperature.

2.2. Preparation of xerogels

Xerogels were prepared, as shown in Table I, by two sol–gel methods: the colloidal gel method (CG) and the polymeric gel method (PG).

In the CG method, the necessary colloidal silica (Degussa, Aerosil 200, industrial quality) to prepare 10 g end product, was dispersed in 100 ml water. During the entire process both stirring and 70 °C temperature conditions were maintained. In Sample 4, NH_4VO_3 (Panreac, for analysis) dissolved in 10 ml 3 M HNO_3 was added to the silica dispersion. Lastly, zirconium (IV) acetate (Aldabó-Julià, industrial quality) dissolved in 100 ml water, was added. When the dispersion was in homogeneous conditions, concentrated ammonia water solution was added drop by drop until gelation occurred at pH = 5, 6.

Likewise, in the PG method, TEOS (Merck, for analysis) (and, in Sample 4, vanadium (IV) oxyacetilacetonate (see Merck, for analysis) necessary for 7 g end product was prehydrolysed for 2 h. The prehydrolysis period was in ethanol in the presence of both water and catalyst (Table II), and maintaining stirring and 70 °C temperature conditions. Then, the necessary amount of zirconium (IV) *n*-propoxide (Fluka, for analysis) was added to the solution and hydrolysed for 24 h (short hydrolysis) or 486 h (long hydrolysis). The solution was then aged and gelled in the open air.

The characteristics of the xerogels achieved, mixture solutions and wet gels are described in Table III. From this table several facts can be deduced: (1) free ZrO_2 (Sample 1) and Samples 2, 3 catalysed by OH^-,

TABLE II Molar ratio conditions

	Molar ratio
$Zr(OPr)_4$: ethanol	1:1.8
$Zr(OPr)_4$: water	1:0.8
$Zr(OPr)_4$: H^+ (or OH^-)	1:0.05

TABLE III Gel characteristics

Composition	Hyd. time (h)	Method	Catalyst	Mixture solution	Gellation time (h)	Wet gel[a]	Dried gel[a]
1	486	PG	H^+	w pp	–	w pp	w trl hom
	24	PG	H^+	w pp	–	w pp	w trl hom
	24	PG	Without	w pp	–	w pp	w op hom
	24	PG	OH^-	w pp	–	w pp	w op hom
2	486	PG	H^+	tr	30	w trl hom	w op hom
	24	PG	H^+	tr	50	w trl hom	w op hom
	24	PG	Without	tr	n.m.	w trl hom	w op hom
	24	PG	OH^-	w pp	–	w pp	w op hom
3	–	CG	–	ye	–	ye op hom	ye op hom
	486	PG	H^+	tr	30	tr nc hom	tr nc hom
	24	PG	H^+	tr	75	tr nc hom	tr nc hom
	24	PG	Without	tr	n.m.	tr nc hom	tr nc hom
	24	PG	OH^-	w pp	n.m.	w pp	tr nc het
4	486	PG	H^+	or/cof	25	or/cof tr hom	or tr hom
	24	PG	H^+	or tr	65	or tr hom	or tr hom
	24	PG	Without	gr tr	n.m.	ye tr hom	ye tr hom
	24	PG	OH^-	gr trl	n.m.	ye tr hom	or trl hom

[a] Colour: nc(colourless), w(white), or(orange), ye(yellow), cof(coffee), gr(green).
Aspect: pp(precipitated), tr(transparent), trl(translucent), hom(homogeneous), het(heterogeneous), op(opaque), n.m.(not measured).

precipitated when *n*-propoxide of zirconium (IV) was added to the mixture; (2) all dried gels obtained appeared homogeneous, except Sample 3, OH^- catalysed, which had an opaque white feature at the bottom and a transparent colourless one on top of the dried gel; (3) samples doped with vanadium were orange or yellow coloured; in the same way, no doped samples were colourless or white; (4) when the hydrolysis time increased, the gellation time decreased significantly.

2.3. Characterization of samples

2.3.1. X-ray diffraction (XRD) and crystallite size measurements

XRD powder diffractograms were obtained using a Philips X-ray diffractometer using nickel and CuK_α radiation. Operating at low speed of the goniometer, the crystallite size was calculated using Scherrer's relationship [9]

$$D = \frac{K\lambda}{\beta \cos\theta} \quad (1)$$

where D is the average crystallite dimension, λ is the X-ray wavelength, β is the full width at half maximum of the peak, θ is the Bragg angle and K is a constant, usually, $K \approx 1$.

2.3.2. DTA–TG measurements

Differential thermal analysis (DTA) and thermogravimetric analysis (TG), were carried out using a Perkin–Elmer instrument in air, with a platinum crucible and a heating time of 20 °C min^{-1}. Finally powdered alumina was used as reference substance.

2.3.3. Infrared (IR) spectroscopy

Infrared spectra of raw samples were obtained using a Perkin–Elmer spectrometer in the range between 4000 and 200 cm^{-1} using the KBr pellet technique.

2.3.4. Vickers microhardness measurements (HV)

In the Vickers test [10], a pyramidal diamond indentor was pressed on to the surface of a metal under a load of W kg and the mean diagonal of the resultant indentation measured (d in mm). The Vickers hardness (HV) number is defined as

$$\mathrm{HV} = \frac{W}{\text{pyramidal area of indentation}} \quad (2)$$

The indentor has an angle of 136° between opposite faces and 146° between opposite edges. From simple geometry, this means that the pyramidal area of indentation is greater than the projected area of the indentation by the radio 1 : 0.9272. Hence

$$\mathrm{HV} = \frac{0.9272\,W}{\text{projected area}} = 1.8544\frac{W}{d^2} \quad (3)$$

The value is expressed in kg mm^{-2}.

2.3.5. Scanning electron microscopy (SEM)–energy dispersion of X-rays (EDX)

Samples were observed by SEM technique in a Hitachi microscope in order to study microstructural features of fractured samples; EDX measurements were taken to determine the semiquantitative evolution of the precise chemical composition.

3. Results and discussion

3.1. XRD and crystallite size measurements

The crystalline phases detected by XRD, the colour of the samples and the crystallite size measured in the samples at each firing temperature tested are shown in Table V. The evolution according to firing temperature of the diffractograms of Sample 3, acid catalyst and 24 h hydrolysis time, are shown in Fig. 1. From

TABLE IV

(a) Crystalline phases, colour and ZrO_2(t) crystallite size (nm) of samples acid-catalysed (HNO_3)

T(°C)	Sample							
	1s	1l	2s	2l	3s	3l	4s	4l
300	A w	A w	A w	A w	A bk	A bk	A bk	A bk
600	M(s) w	M(s)T(m) w/31	A w	A w	A bk	A bk	A bk	A bk
750	M(vs) w	M(vs) w	T(w) w/13	T(m) w/20	T(w) bk/18	T(m) bk/18	T(w) bk/18	T(vw) bk/11
800	M(vs) w	M(vs) w	T(s) w/17	T(w) bk/19	T(w) bk/19	T(m) bk/18	T(w) bk/18	T(w) bk/11
900	M(vs) w	M(vs) w	T(s) w/17	T(s) bk/15	T(s) bk/15	T(s) bk/15	T(m) bk/14	T(m) ye/12
1000	M(vs) w	M(vs) w	T(vs) w/23	T(vs) w/26	T(s) bk/18	T(s) bk/22	T(vs)M(w) Z(vw) gr/46	Z(vs) gr
1100	M(vs) w	M(vs) w	T(vs)M(w) w/46	M(m)T(w) w/37	T(vs)M(w) w/46	T(vs)M(w) w/46	Z(vs) gr-bl	Z(vs) gr-bl
1200	M(vs) w	M(vs) w	M(s)Z(vw) w	M(s)Z(vw) w	T(s)M(s) w	T(s)M(w) w/61	Z(vs) bl-gr	Z(vs) bl-gr
1400	M(vs) w	M(vs) w	M(m)Z(s) w	M(s)Z(s) w	M(vs)T(w) Z(m)C(w) w	M(m)T(w) C(m) w	Z(vs) bl	Z(vs) bl

(b) Crystalline phases, colour and ZrO_2(t) crystallite size (nm) of base (NH_3) and uncatalysed samples

T(°C)	Sample									
	1b	1n	2b	2n	3b	3n	3CG	4b	4n	4CG
300	A w	A w	A w	A w	A w	A w	–	A bk	A bk	–
600	T(s)M(w) w/24	T(w)M(w) w/39	A w	A w	A w	A w	–	A bk	A bk	T(s) gr-bl/14
750	M(s)T(w)	T(s)M(m) w/30	T(s) w/20	A w	T(w) bk/17	T(s) bk/22	– –	T(w) ye/12	A bk	T(vs) ye/12
800	M(vs)T(w) w/37	T(s)M(s) w/46	T(s) w/12	T(s) w/12	T(m) gy/17	T(s) bk/23	T(s)M(w) w/23	T(m) ye/14	A bk	T(s)M(w) ye/20
900	M(vs) w	T(vs) w/46	T(s) w/18	T(s) w/18	T(s) gy/15	T(s) bk/20	T(s)M(vw) w/31	T(vs) gr/17	T(m) bk/13	Z(vs)M(w) C(vw) bl-gy
1000	M(vs) w	M(vs) w	T(s) w/23	T(s) w/23	T(vs) gy	T(vs) bk/23	T(s)M(vw) w/31	Z(vs) gr	Z(vs) gr-bl	Z(vs)M(w) C(vw) bl-gy
1100	M(vs) w	M(vs) w	T(s)M(w) w/35	T(s)M(s) w/44	T(vs)M(w) w/35	T(vs)M(w) gy/44	–	Z(vs) gr-bl	Z(vs) bl-gr	Z(vs)M(w) C(vw) bl-gr
1200	M(vs) w	M(vs) w	M(vs) w	M(s) w	T(vs)M(w) w	T(m)M(m) w/52	T(s)M(m) w	Z(vs) bl-gr	Z(vs) bl-gr	Z(vs) bl
1400	M(vs) w	M(vs) w	M(s)Z(m) C(w) w	M(vs) w	M(m)Z(s) C(m) w	M(s)Z(s) T(w)C(m) w/46	Z(vs)T(w) M(vw) w/61	Z(vs) bl-gr	Z(vs) bl-gr	–

Crystalline phases: $MZrO_2$(t); $TZrO_2$(m); C, cristobalite; Z, zircon; A, amorphous. Peak intensity: v, very; s, strong; m, medium; w, weak. Hyd. time: short hydrolysis, 24 h (s), and long hydrolysis 486 h (l). Colour of samples: w, white; bk, black; ye, yellow; gr, green; bl, blue; gy, grey.

TABLE V DTA–TG results

Sample	Catalyst	Hyd time (h)	EN (solv)[a]	EX (org)[a]	EX (cryst)	% TG[b]	XRD[c]	Colour
1	HNO_3	24	159(m)	444(s)	–		M(m)	White
2		"	160(m)	277(m) 390(w)	858(w)		T(m)	White
3		"	140(m)	295(w) 429(w)	896(w)	71.5	T(m)	White
4		"	156(m)	245(m)	897(w)	69.8	T(w)	Black
1	HNO_3	486	155(m)	376(w) 453(s)	–		M(s)	White
2		"	154(m)	295(m) 521(w)	830(w)		T(m)	White
3		"	181(m)	320(w) 493(w)	910(w)	71.5	T(m)	Black
4		"	142(m)	301(m)420(s)	744(w)	73.9	T(s)	Black
1	OH^-	24	152(m)	461(s)	–		M(s)	White
2		"	149(m)	329(w)	880(w)		T(s)	White
3		"	155(m)	583(vw)	899(vw)		T(m)	Black
4		"	146(w)	337(w)	724(m)	70.8	T(s)	Black
1	Without	24	156(m)	461(s)	–		M(s)	White
2		"	154(m)	–	865(m)		T(m)	White
3		"	153(m)	447(m)	927(vw)		T(m)	White
4		"	150(m)	405(w)	892(w)	73.3	T(m)	Black
3	CG	CG	130(w) 250(w)	314(w) 363(w)	540(w) 1020(w)	51.7	Z(s)M(w)	Green

[a] EX, DTA exothermic peak; EN, DTA endothermic peak; solv, solvent evaporation; org, combustion of organics; cryst, crystallization.
[b] % TG, % weight after TG.
[c] Intensity of peaks: vw, very weak; w, weak; m, medium; s, strong; vs, very strong.

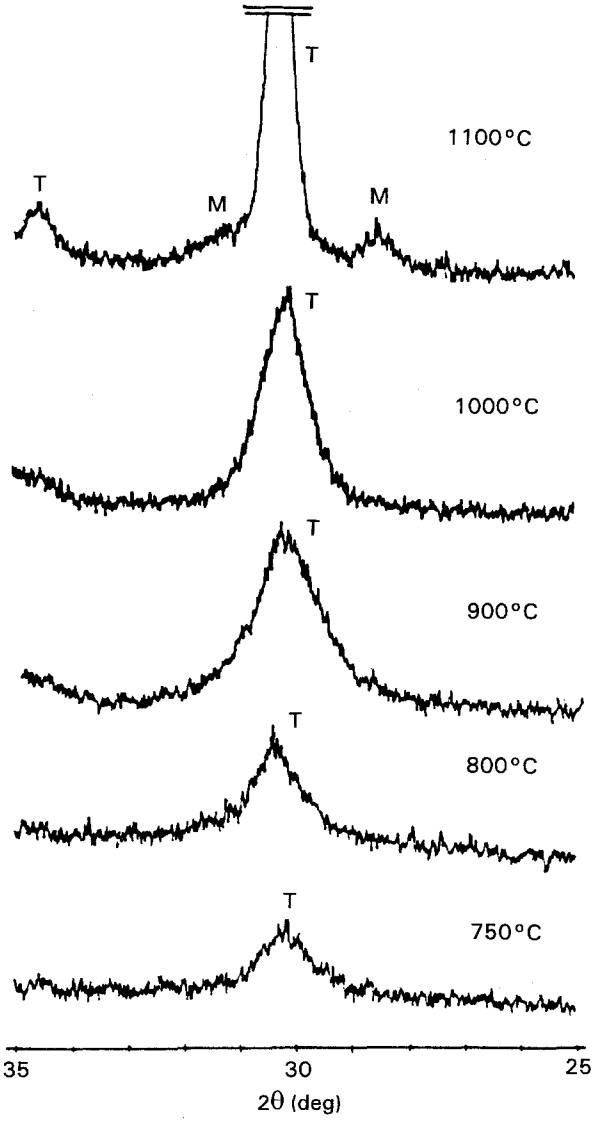

Figure 1 Evolution of XRD patterns with temperature. Crystalline phases: T, ZrO_2(t); M, ZrO_2(m).

results in Table V we can discuss several facts: nucleation temperature of the different crystalline phases; range of thermal stability of ZrO_2(t)–silica composites; the ZrO_2(t) crystallite size evolution; and colour evolution of the samples.

3.1.1. Nucleation temperature

As a rule, the crystalline phase evolution, amorphous → ZrO_2(t) → ZrO_2(t) and ZrO_2(m) → $ZrSiO_4$ and/or (ZrO_2(t) and ZrO_2(m)) and/or cristobalite, is observed in all samples, independently of either catalyst or method of preparation of gels. The dividing lines in Table IV indicate the test temperatures at which ZrO_2(m) $ZrSiO_4$ phases are respectively nucleated.

The nucleation of ZrO_2(t) is observed around 750 °C in most parts of the samples. Free ZrO_2 and CG samples nucleate at lower temperatures [11], because their lower scale of homogeneity (around 1 μm colloidal particles in the CG method and similar or higher values of free ZrO_2 precipitated particles). In this sense it should be noticed that Samples 2 and 3 (OH^- catalysed), show a common behaviour in spite of their precipitated aspect, this fact, together with the heterogeneous aspect of the gel in Sample 3 indicates that in these samples total precipitation has not been achieved, and particles of ZrO_2 and SiO_2 are not separated as in samples 1 and GC samples.

The range of ZrO_2(t) in amorphous matrix composite stability exhibits a similar feature. It does not appear in Sample 1 and it is narrow in GC and vanadium-doped samples (Samples 4). On the other hand, Samples 2 and 3 show thermal stability of this composite between 750 and 1000 °C; at 1100 °C ZrO_2(m) is always detected. The polyphasic ZrO_2(m) and ZrO_2(t) in a silica matrix composite shows a similar range of stability, but in Sample 3 it is wider than

in Sample 2, where zircon is detected or ZrO_2(t) disappears at 1200 °C. Likewise in Samples 4, vanadium seems to promote zircon nucleation and this phase is detected at 1200 °C.

Generally, it can be observed that the crystalline phase evolution is more influenced by the chemical composition than by the catalyst employed. However, in free ZrO_2 samples (Samples 1), acid catalyst strongly reduces the range of ZrO_2(t) stability and, on the other hand, base catalyst seems to favour crystallization of ZrO_2(t) faster than acid catalyst, and systems without catalyst (samples 2N and 4N exhibit a relatively wide amorphous range). In this sense, the silica content enlarges the thermal stability of the ZrO_2(t) phase, and vanadium doping promotes ZrO_2(t) nucleation. These results agree with previous reports [11, 12].

3.1.2. ZrO_2(t) crystallite size evolution

The ZrO_2(t) crystallite size measured at each firing temperature is shown in Table IV. From these results, it can be observed that in the range of ZrO_2(t)–amorphous matrix composite stability, the size of the ZrO_2(t) crystallite is lower than 30 nm, when the crystallite grows, ZrO_2(t) → ZrO_2(m) takes place, therefore, according to the literature [7], in both free ZrO_2 and ZrO_2(t)–SiO_2 composites, the critical particle size for ZrO_2(t) → ZrO_2(m) transformation is around 30 nm. This value does not seem to be affected significantly by the catalyst system, hydrolysis time or the gel method used.

3.1.3. Colour evolution of the samples

Samples 1 and 2 remain white after all thermal treatment steps. Samples 3 become black at low firing temperatures, but at around 800 °C turn white in colour. Samples 4 are also black at low temperatures, but turn yellow when ZrO_2(t) phase develops and, when $ZrSiO_4$ crystallizes, they become green–blue coloured. Finally, the blue colour is enhanced in the samples. The CG sample is not initially black and no bluish evolution of colour is observed at high firing temperatures.

The black colour of the samples is associated with the residual carbon from organic precursors. Carbon remains encapsulated in the amorphous matrix generated by heating of the xerogel. When the temperature increases, it is burned up. Several authors thought that this trapped carbon promoted the ZrO_2(t) stabilization [13]. In this case, the trapped carbon (indicated by the black colour), does not seem to have a significant effect on ZrO_2(t) stability.

Not all white coloured samples look alike; base samples and samples without catalyst present a dull white colour, while acid-catalysed samples look nacred in the range 750–1100 °C. They then lose brightness coinciding with the detection of $ZrSiO_4$ as the predominant crystalline phase.

3.2. DTA and TG–DTG analysis

DTA and TG–DTG curves of both PG (3, acid catalyst, 24 h hydrolysis time) and CG (4) samples are drawn in Fig. 2.

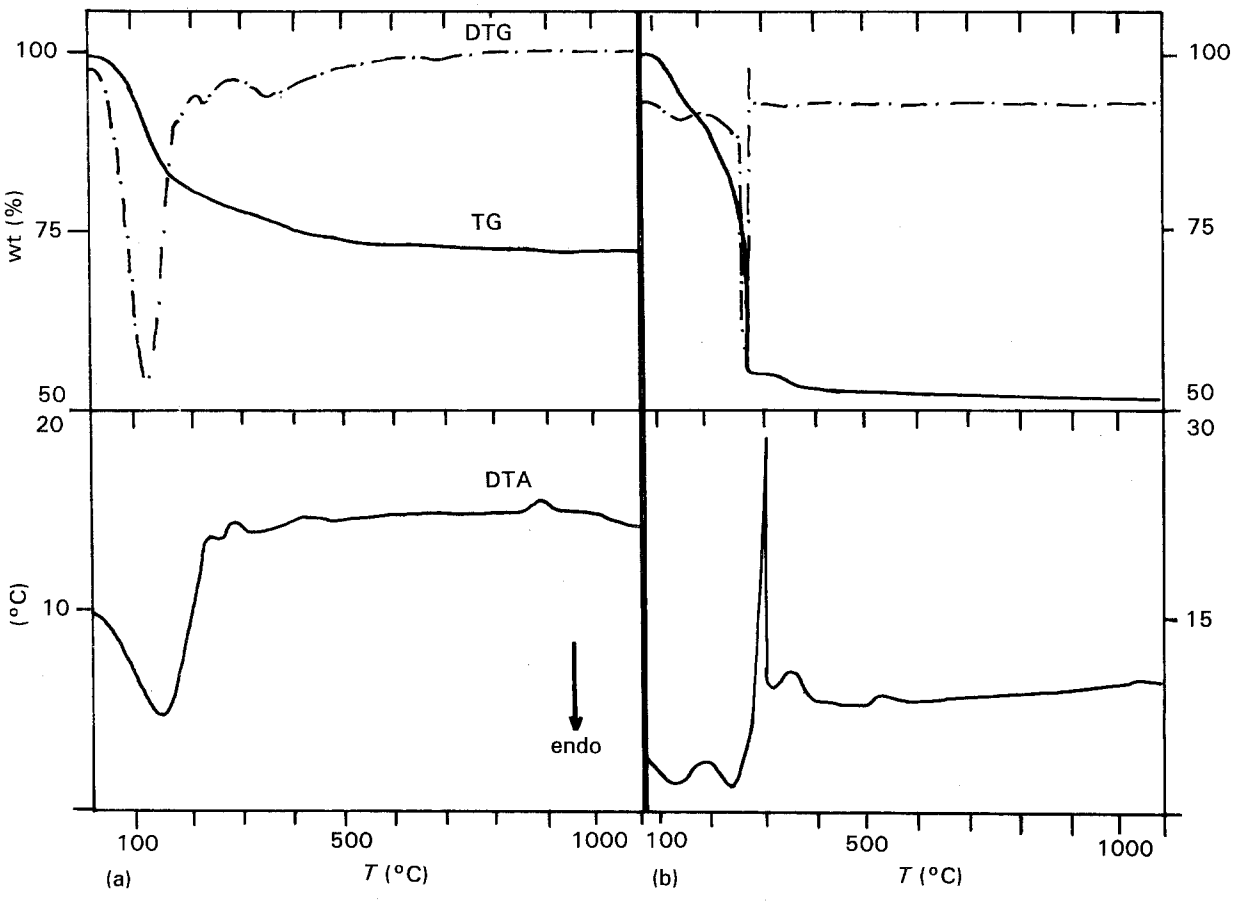

Figure 2 DTA and TG–DTG curves of samples. (a) Sample 3, PG, acid catalyst, short hydrolysis. (b) Sample 4, CG.

DTA results from tested samples, together with the crystalline phases detected in the residual samples and TG–DTG results, are presented in Table V. It is observed that ZrO_2(t) crystallization is always detected by a weak exothermic peak between 720 and 920 °C; this wide dispersion of values seems to have no significance when they are compared with XRD data in Table IV. Likewise ZrO_2(m) can be associated with the brittle look of residual Sample 4, and ZrO_2(t) with the hard appearance of Samples 2, 3 and 4.

Free ZrO_2 samples show a strong exothermic peak at $\sim$ 450 °C which is associated with entrapped organic group combustion; the rest of the samples exhibit this peak with lower intensity and temperature. This fact can be associated with the white colour observed in the residual sample. Likewise Sample 2 remains white in contrast to Samples 3 and 4 which are black. As mentioned above, the black colour is due to residual carbon from organics which remain entrapped in the monolithic fired gel. In this sense, samples with low SiO_2 content do not present an efficient encapsulation of carbon, in contrast with Samples 3 and 4 which entrap carbon easily, independently of the catalyst system. In this way these results agree with the colour evolution of the samples discussed above.

TG–DTG measurements also agree, according to DTA results. There is a loss of weight associated with either solvent evaporation or organic combustion but no loss is detected at ZrO_2(t) crystallization temperature. The residual weight in all PG samples after TG treatment is around 72%, and 50% in the CG sample. The feature of the TG curves indicates that in CG samples, organic loss is stronger according to the residual weight observed in these samples.

3.3. IR spectroscopy

The IR spectra of Samples 3 obtained by the PG method, catalysed by acid and treated with 24 and 486 h hydrolysis time (short and long hydrolysis, respectively), and Sample 4 CG, are shown in Fig. 3. IR band assignation made on the spectra which ran between 4000 and 200 cm^{-1} is drawn out in Table VI. From these results, several facts can be depicted.

(a) The band around 620 cm^{-1} associated with ZrO_8 [7] group is not detected in samples without catalyst.

(b) The bands around 966 cm^{-1} associated with $Si–O^-$ bonds (O^- signifying non-bridging oxygen ions) [7] appears strong in all samples except the CG sample where a strong band at 1100 cm^{-1} associated with Si–O bonds is detected.

(c) From the bands at 774 and 457 cm^{-1}, respectively, which can be associated with Si–O–Si bonding [7], only a weak band at 457 cm^{-1} normally appears; the 774 cm^{-1} band is detected only on Sample 4 base catalysed and in the CG sample. The Zr–O group throbs in baddeleyite at 749, 496 and 411 cm^{-1} [14]; this band system is not detected, even in samples without catalyst which do not present the band associated with the ZrO_8 group.

(d) All samples present a band around 1380 cm^{-1} which can be associated with the NO_3^- group; however, this band also appears in samples without HNO_3 addition, hence, it must be associated with ZrO^- bonds in hydrolysed zirconium (IV) *n*-propoxide.

Therefore, it must be concluded that in xerogels prepared by the polymeric gel method, no Si–O–Si network is achieved. On the other hand, zirconium–oxygen seems not to be bonded, as in baddeleyite. Therefore, if either Si–O–Si or ZrO_2 networks are not detected, it must be thought that hydrolysed SiO^- and ZrO^- bonds built a kind of nanocomposite where the silicon atom and other silicons or zirconiums are separated by a residual sphere of organic

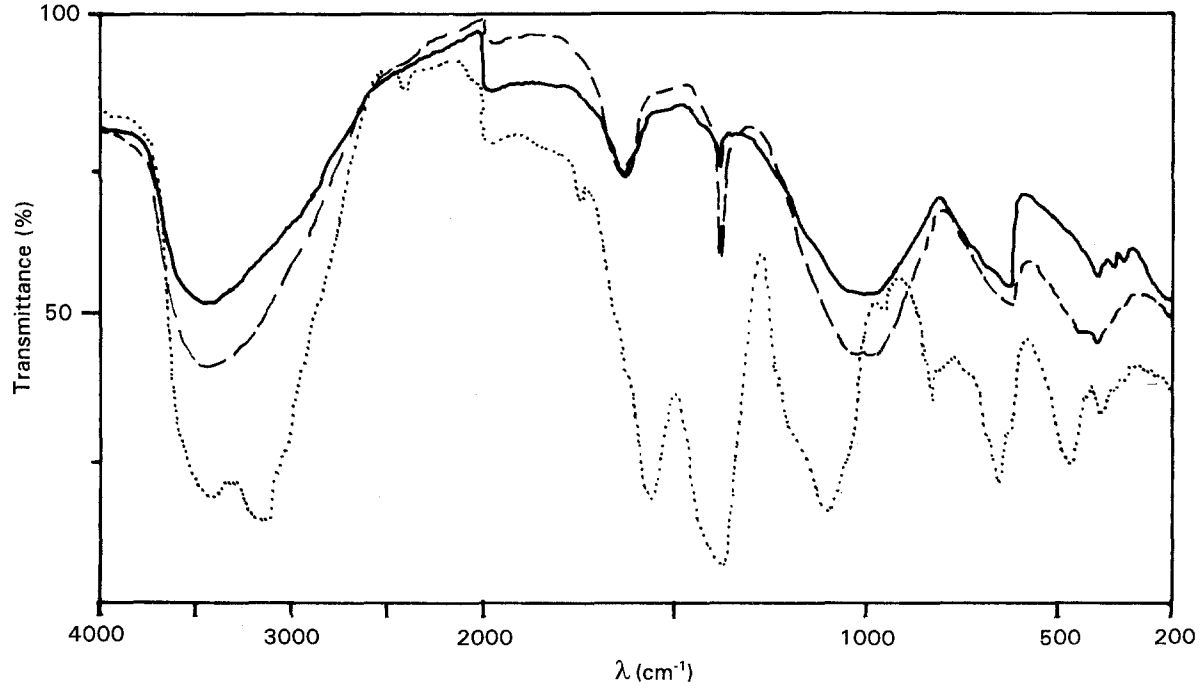

Figure 3 IR spectra of samples. (——) Sample 3, PG, acid catalyst, long hydrolysis, (– – –) Sample 3, PG, acid catalyst, short hydrolysis; (- - -) Sample 4, CG.

TABLE VI IR bands (cm^{-1}) assignation from raw samples spectra

Sample	O–H/H_2O	Si–O	Si–O^-	Si–O–Si	V–O	Zr–O	ZrO_8	Zr–O^-	Others
Literature [7, 10, 14]	3400, 1600	1079	966	774, 457	3215, 1401, 965, 732, 600 399, 346	740, 500, 411	620	1380	
1, s, H^+	3428, 1615	–	–	–	–	444, 388	620	1371	
1, l, H^+	3424, 1604	–	–	–	–	416, 398	–	1371	364, 348
2, s, H^+	3416, 1625	1000	957	445	–	445	642	1370	2400, 550
2, l, H^+	3398, 1607	–	959	–	–	416, 318	606	1371	
3, s, H^+	3415, 1616	1000	960	470	–	415, 322	606	1369	341
3, l, H^+	3385, 1618	–	964	–	–	409	601	1370	
4, s, H^+	3386, 1610	1017	950	496	–	411	615	1369	
4, l, H^+	3411, 1609	1007	968	–	–	402, 318	601	1371	
1, s, OH^-	3416, 1560	–	–	458	–	458, 373	650	1366	
2, s, OH^-	3400, 1623	–	977	431	–	–	603	1383	
3, s, OH^-	3389, 1618	1008	969	417	–	389	629	1384	
4, s, OH^-	3397, 1624	–	980	761, 458	–	433, 390	608	1386	372, 313
1, s, w	3415, 1557	–	–	–	–	418	607	1360	321
2, s, w	3410, 1619	–	963	444	–	391	–	1382	
3, s, w	3397, 1624	–	983	440	–	391	–	1382	
4, s, w	3414, 1622	–	981	428	–	389	–	1381	
4, CG	3420, 1545	1100	950	820, 461	–	385	606	1391	2001, 3128 335, 1742

[a] s, short hydrolysis, 24 h; l, long hydrolysis; 486 h, H^+, acid hydrolysis, OH^-, base hydrolysis; w, without catalyst; CG, colloidal gel.

TABLE VII Vickers microhardness measurements

Sample	Firing temp. (°C)	Load (g)	HV (kg/mm^{-2})	XRD phases[b] and cryst. size (nm)
2, s, H^+	750	100	532.4	T(w)/13
		500	533.9	
3, s, H^+		100	287.5	T(w)/18
		500	298.6	
4, s, H^+		100	358.1	T(w)/18
		500	438.8	
2, l, H^+		100	552.2	T(m)/20
		500	596.4	
3, l, H^+		100	577.4	T(m)/18
		500	648.9	
4, l, H^+		100	580.0	T(vw)/11
		500	549.5	
2, s, H^+	1100	100	245.5	T(vs)M(w)/46
		500	268.6	
2, s, OH^-		100	274.6	T(s)M(w)/35
2, s, w		100	324.8	T(s)M(w)/44
3, s, H^+		100	660.6	T(vs)M(vw)/41
		500	675.9	
2, l, H^+		100	728.0	T(w)M(m)/37
		500	788.0	
3, l, H^+		100	707.3	T(s)M(w)/61
		500	675.4	

[a] s, short hydrolysis, 24 h; l, long hydrolysis, 486 h; H^+, acid hydrolysis; OH^-, base hydrolysis; w, without hydrolysis.
[b] Crystalline phases: M, M-ZrO_2; T, T-ZrO_2; Peak intensity: v, very; s, strong; m, medium; w, weak.

and OH groups. In any case, no direct evidence of Si–O–Zr bonds has been detected, but this bond cannot be discounted from the IR bands shown by the samples.

3.4. Vickers microhardness measurements

Table VII shows the results obtained by Vickers microhardness tests using identation loads of 100 and 500 g. The positive effect of hydrolysis time on microhardness is clearly seen; long hydrolysis time enhances significantly the Vickers values. Other parameters such as crystalline phase composition, ZrO_2(t) crystallite size and catalyst used do not significantly affect microhardness values.

It should be noted that in these samples with a long hydrolysis time, the IR band at 457 cm^{-1} associated with Si–O–Si bonds is not detected; a more adequate raw nanocomposite must be built in order to obtain better mechanical properties.

3.5. Scanning electron microscopy and energy dispersion analysis (EDX)

Several micrographs of significant samples are shown in Fig. 4. Testing superficial microstructure by SEM, gives rise to the following remarks.

(a) All samples present a monolithic feature under temperatures of zircon crystallization (Fig. 4a, b). When zircon crystallizes, the surface becomes porous in Samples 4 (a and e). In other samples, a granulated or rough surface is observed but without porosity.

(b) All samples present a very neat plane of fracture (cracks). However, together with these fractures (when zircon crystallizes), other irregular bent cracks associated with porosity appear (c and d).

(c) SEM does not indicate microstructural differences among samples synthesized by different hydrolysis times which could explain the different behaviour in the microhardness tests (Fig. 4b–e, and c and d). Likewise, no differences were detected among samples from different catalyst systems (b, f, g).

EDX analysis carried out on Samples 3 shows a homogeneous composition either in the flat surface or in the fracture area or in small particles pulled out during cracking (Fig. 4c and g). However, in Sample 4,

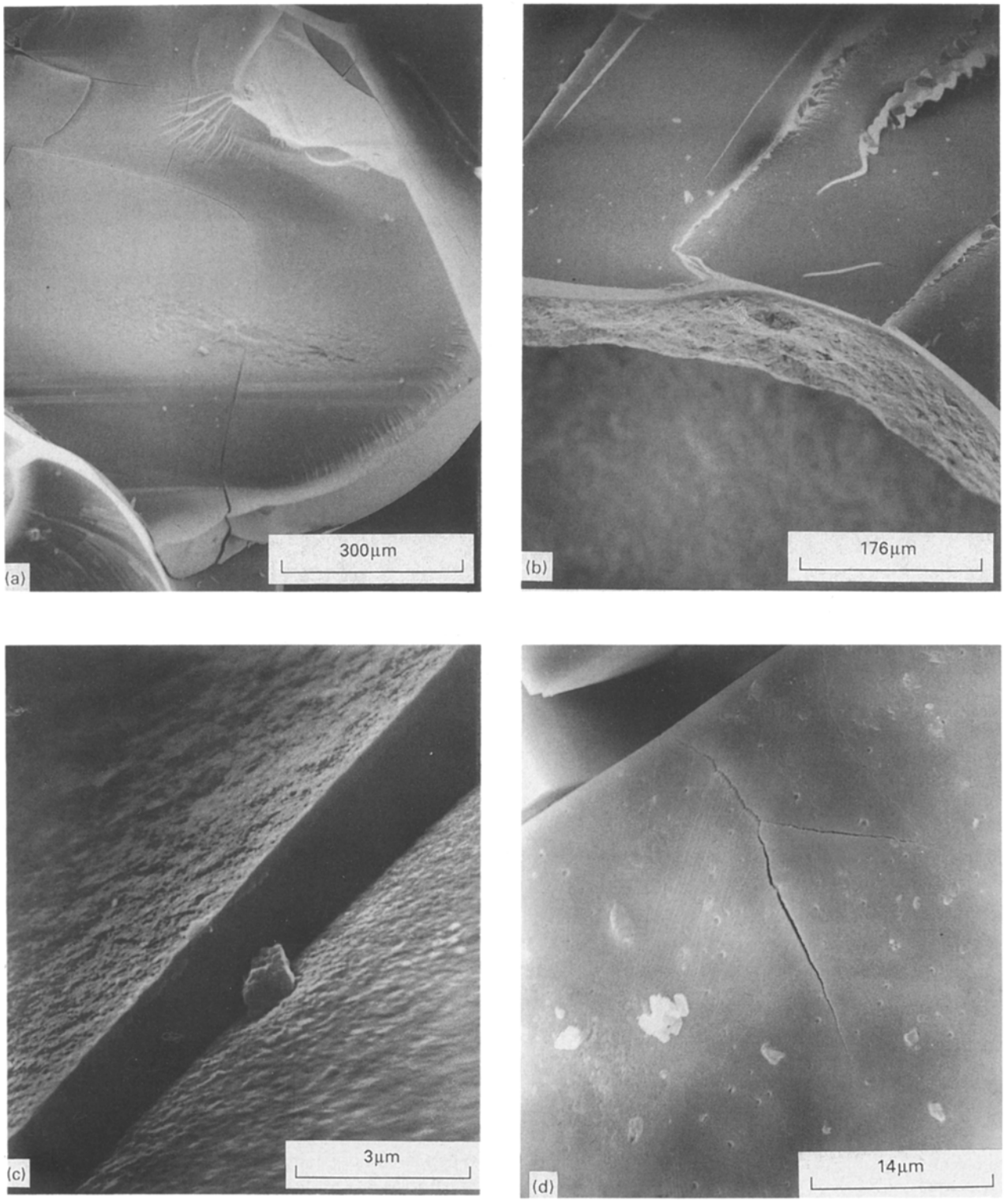

Figure 4 Scanning electron micrographs. (a) Sample 1, acid catalyst, short hydrolysis, 1000 °C/12 h; (b) Sample 3, acid catalyst, short hydrolysis, 1000 °C/12 h. (C) Sample 4, acid catalyst, long hydrolysis, 900 °C/12 h. (d) Sample 4, acid catalyst, short hydrolysis, 1000 °C/12 h. (e) Sample 4, acid catalyst, short hydrolysis, 1400 °C/12 h. (f) Sample 3, acid catalyst, long hydrolysis, 1000 °C/12 h. (g) Sample 3, without catalyst, short hydrolysis, 1000 °C/12 h. (h) Sample 3, base catalyst, short hydrolysis, 1000 °C/12 h.

there are many superficial particles associated with porosity (Fig. 4d) which turns out to be free V_2O_5 particle from EDX analysis.

4. Conclusions

From the above discussion, the following conclusions may be drawn.

1. Either from gels obtained by the sol–gel process from aqueous solution (CG gels) or gels from the hydrolysis– condensation alkoxides process (PG), it is possible to stabilize the ZrO_2 tetragonal polymorph even after annealing at 1400 °C/12 h.

2. In the PG method, the catalyst used and the hydrolysis time of the alkoxide mixtures do not seem to influence the range of temperature over which the

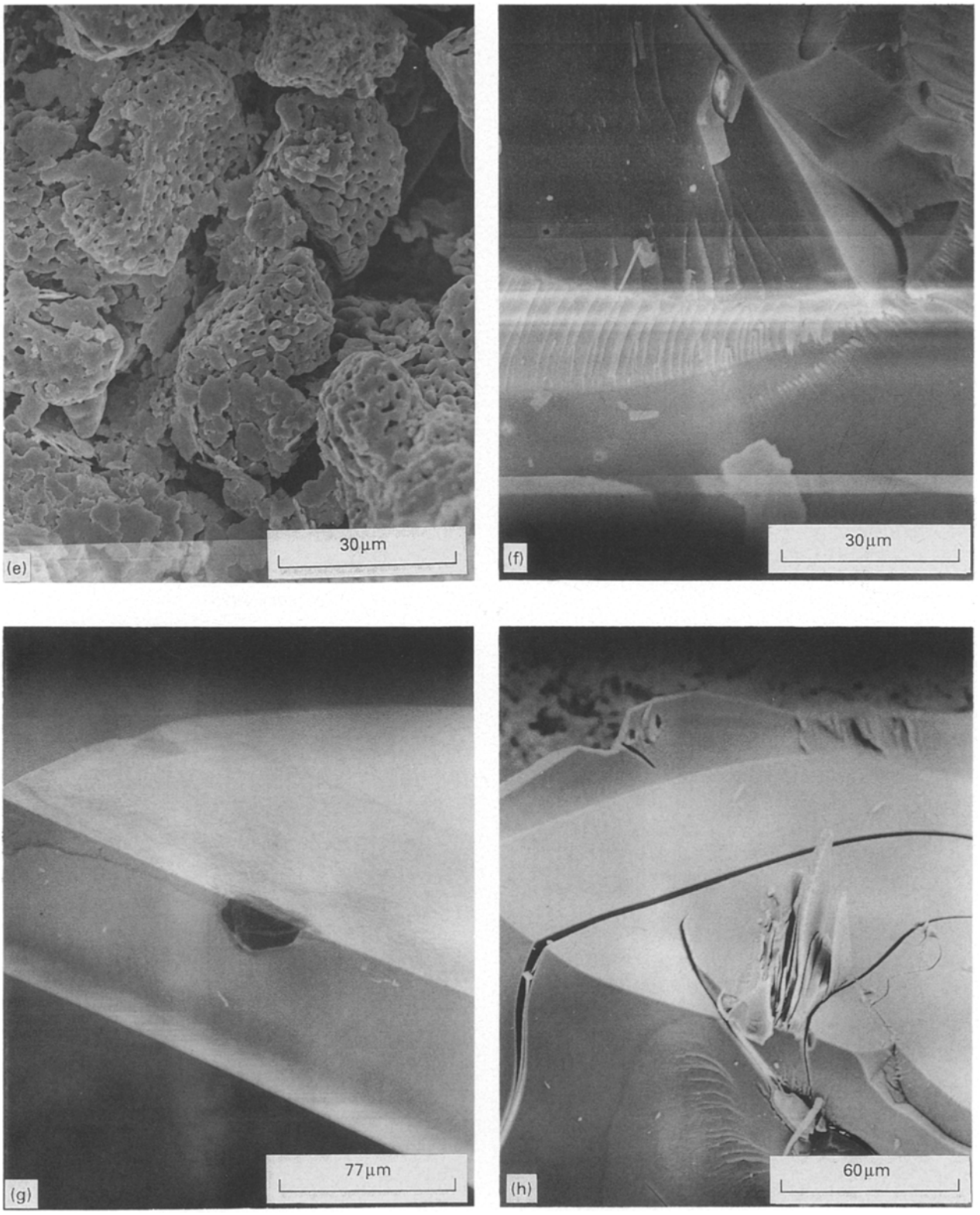

Figure 4 continued.

tetragonal ZrO_2 in the SiO_2 matrix glass-ceramics composite is stable. However, the chemical composition affects it seriously: $SiO_2 \cdot ZrO_2$ composition presents a wider range of stability, and a decrease in SiO_2 content or doping with vanadium gives rise to a narrow range, finally, a free ZrO_2 sample catalysed by HNO_3 does not stabilize this composite.

3. Instabilization of ZrO_2(t)–SiO_2 glass-ceramic composite occurs when crystallites of ZrO_2(t) reach a critical size around 30 nm, and the martensitic transformation ZrO_2(t) to ZrO_2(m) occurs.

4. Vickers microhardness tests show a hardness increase in ZrO_2(t) –SiO_2 composites from PG samples with a long hydrolysis time. SEM studies do not

indicate significant differences between long and short hydrolysis times, only IR spectra show that in long hydrolysis samples, the 457 cm^{-1} band assigned to Si–O–Si bonds is not detected.

5. SEM–EDX does not indicate differences in the monolithic microstructure in glass-ceramic samples; when zircon crystallizes, free V_2O_5 crystals associated with a porous surface are detected in samples doped with vanadium (Sample 4) and become porous at 1400 °C.

Acknowledgements

The authors thank "Servei de Microscopia Electrònica de la Universitat de València" for their help in SEM-EDX analysis, and the "Universitat Jaume I de Castelló-Fundació Caixa Castelló", for financial support for the project CE.25.015/92 which made this paper possible.

References

1. R. W. RICE, *Mater. Res. Soc. Symp. Proc.* **32** (1984) 337.
2. R. J. HILL and B. E. REICHERT, *J. Am. Ceram. Soc.* **73** (1990) 2822.
3. R. C. GARVIE, R. H. HANNICK and R. T. PASCOE, *Nature (London)* **258** (1975) 703.
4. T. K. GUPTA, F. F. LANGE and J. H. BECHTOLD, *J. Mater. Sci.* **13** (1978) 1464.
5. A. H. HEUER, N. CLAUSSEN, V. M. KRIVEN and M. RÜHLE, *J. Am. Ceram. Soc.* **65** (1982) 642.
6. P. MIRANZO, P. PENA, S. DE AZA, J. S. MOYA, J. Ma. RINCON and G. THOMAS, *J. Mater. Sci.* **22** (1987) 2987.
7. M. NOGAMI, *J. Non-Cryst. Solids* **69** (1985) 415.
8. M. NOGAMI and M. TOMOZAWA, *J. Am. Ceram. Soc.* **69** (1986) 99.
9. L. BRAGG, in "Handbook of X-Ray", edited by Emmett and F. Kaeble (1967) Ch. 17, p. 1.
10. D. E. GRAY, in "American Institute of Physics Handbook", 3rd Edn (McGraw-Hill, New York, 1972) Ch. 2, p. 79.
11. G. MONROS, J. CARDA, P.ESCRIBANO and J. ALARCON, *J. Mater. Sci. Lett.* **9** (1990) 184.
12. V. S. NAGARAJAN and K. J. RAO, *J. Mater. Sci.* **24** (1989) 2140.
13. A. SAMDI, T. GROLLIER BARON, B. DOURAND and M. ROUBIN, *Ann. Chim. Fr.* **13** (1988) 171.
14. G. MONROS, J. CARDA, P. ESCRIBANO and J. ALARCON, *Br. Ceram. Trans. J.* **90** (1991) 157.

Received 3 July 1992
and accepted 24 February 1993